JACS
JOURNAL OF THE AMERICAN CHEMICAL SOCIETY
Article
pubs.acs.org/JACS

Aluminum-Phosphate Binder Formation in Zeolites as Probed with X-ray Absorption Microscopy

Hendrik E. van der Bij,[†] Dimitrije Cicmil,[†] Jian Wang,[‡] Florian Meirer,[†] Frank M. F. de Groot,[†] and Bert M. Weckhuysen*[,†]

[†]Inorganic Chemistry and Catalysis group, Debye Institute for Nanomaterials Science, Utrecht University, 3584 CG Utrecht, The Netherlands

[‡]Canadian Light Source, Inc., University of Saskatchewan, Saskatoon, Saskatchewan S7N 2V3, Canada

Supporting Information

ABSTRACT: In this work, three industrially relevant zeolites with framework topologies of MOR, FAU and FER have been explored on their ability to form an $AlPO_4$ phase by reaction of a phosphate precursor with expelled framework aluminum. A detailed study was performed on zeolite H-mordenite, using in situ STXM and soft X-ray absorption tomography, complemented with ^{27}Al and ^{31}P magic angle spinning nuclear magnetic resonance (MAS NMR) spectroscopy, XRD, FT-IR spectroscopy, and N_2 physisorption. Extraframework aluminum was extracted from steam-dealuminated H-mordenite and shown to dominantly consist of amorphous AlO(OH). It was found that phosphoric acid readily reacts with the AlO(OH) phase in dealuminated H-mordenite and forms an extraframework amorphous $AlPO_4$ phase. It was found that while $AlPO_4$ crystallizes outside of the zeolitic channel system forming $AlPO_4$ islands, $AlPO_4$ that remains inside tends to stay more amorphous. In the case of ultrastable zeolite Y the FAU framework collapsed during phosphatation, due to extraction of framework aluminum from the lattice. However, using milder phosphatation conditions an extraframework $AlPO_4$ α-cristobalite/tridymite phase could also be produced within the FAU framework. Finally, in steamed zeolite ferrierite with FER topology the extraframework aluminum species were trapped and therefore not accessible for phosphoric acid; hence, no $AlPO_4$ phase could be formed within the structure. Therefore, the parameters to be taken into account in $AlPO_4$ synthesis are the framework Si/Al ratio, stability of framework aluminum, pore dimensionality and accessibility of extraframework aluminum species.

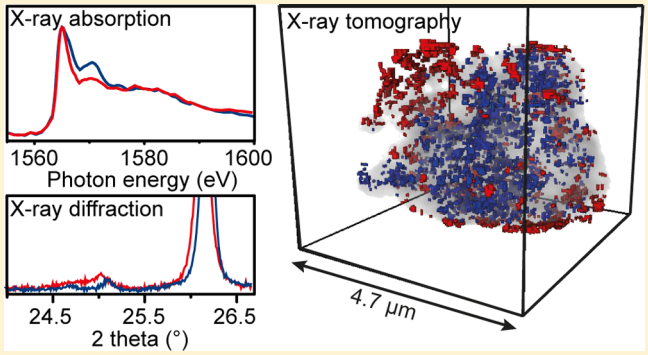

INTRODUCTION

Catalysis performed over the crystalline microporous aluminosilicates known as zeolites is of enormous importance to the oil and gas industry as their use saves (petro)chemical companies billions of dollars in process and energy costs.[1] Because of their wide and valuable application range in catalytic cracking and potential use in, e.g., catalytic fast pyrolysis of biomass, (bio)alcohol dehydration and (bio)alcohol conversion to hydrocarbons, there is a great academic interest in zeolites as heterogeneous catalysts.[2−7] However, as was recently pointed out in two reviews, the academic world focuses strongly on the performance of pure zeolite materials, while in industry the application of binders and matrices, used in catalyst bodies to increase mechanical strength and attrition resistance, exert a huge influence on performance as well.[8,9]

An example of the interaction between binder and zeolite is aluminum-phosphate ($AlPO_4$). Especially in the field of catalytic hydrocarbon cracking, the addition of $AlPO_4$ to zeolites, often in combination with a zeolite phosphatation step, leads to improved light olefin selectivity, hydrothermal stabilization, improved mechanical strength and attrition resistance.[10−14] Furthermore, it has been shown that $AlPO_4$ can form from a zeolite's own aluminum supply by applying a dealumination and subsequent phosphorus modification (phosphatation) step.[15−19]

The formation of an $AlPO_4$ binder by using part of the framework aluminum supply is an interesting method for multiple reasons. First, it requires zeolites with high aluminum content, which are cheaper and more environmentally friendly to produce, since the use of organic templates is not required.[20,21] Second, the predealumination step leads to the formation of mesopores, creating a hierarchical material, facilitating access to reactant and product molecules during catalysis.[22,23] And third, a thorough understanding of the formation of $AlPO_4$ from extraframework aluminum ($\{Al\}_{EF}$) should allow one to form $AlPO_4$ species inside the zeolite channel/cage system, altering its shape selective properties.[24]

However, the exact nature of this $AlPO_4$ phase has not yet been studied in great detail. Corma and co-workers found that

Received: August 26, 2014
Published: November 21, 2014

   dx.doi.org/10.1021/ja508545m | J. Am. Chem. Soc. 2014, 136, 17774−17787

Table 1

sample[a]	parent	treatment	sample	parent	treatment
CBV 21A (NH_4-mordenite)	–	–	CBV 500 (NH_4–USY)	–	–
[MOR]	CBV 21A	Calcined 550 °C, 10 h	[USY]	CBV 500	Calcined 550 °C, 10 h
$[MOR]_{400}$	[MOR]	Steamed 400 °C, 4 h	$[USY]_{P\text{-}ST}$	[USY]	Refluxed in HNO_3 and H_3PO_4, dried, steamed 600 °C, 2 h
$[MOR]_{400\text{-}P}$	$[MOR]_{400}$	Refluxed in HNO_3 and H_3PO_4, dried	$[USY]_{P\text{-}WI\text{-}ST}$	[USY]	Wet impregnation H_3PO_4, dried, steamed 600 °C, 2 h
$[MOR]_{400\text{-}P\text{-}ST}$	$[MOR]_{400\text{-}P}$	Steamed 470 °C, 2 h	CP914 (NH_4-ferrierite)	–	–
$[MOR]_{400\text{-}L}$	$[MOR]_{400}$	Leached with HNO_3, filtered, dried	[FER]	CP914	Calcined 550 °C, 10 h
$[MOR]_{400\text{-}L\text{-}P\text{-}ST}$	$[MOR]_{400\text{-}L}$	Refluxed in HNO_3 and H_3PO_4, dried. Steamed 470 °C, 2 h	$[FER]_{500}$	[FER]	Steamed 500 °C, 4 h
Filtrate	$[MOR]_{400\text{-}L}$	Filtrate obtained from leaching	$[FER]_{500\text{-}P}$	$[FER]_{500}$	Refluxed in HNO_3 and H_3PO_4, dried
Filtrate + P	Filtrate	H_3PO_4, dried, steamed 600 °C, 2 h	$[FER]_{500\text{-}P\text{-}ST}$	$[FER]_{500\text{-}P}$	Steamed 600 °C, 2 h
			$[FER]_{600}$	FER	Steamed 600 °C, 4 h
			$[FER]_{600\text{-}P}$	$[FER]_{600}$	Refluxed in HNO_3 and H_3PO_4, dried
			$[FER]_{600\text{-}P\text{-}ST}$	$[FER]_{600\text{-}P}$	Steamed 600 °C, 2 h

[a]Abbreviations: ST = steam treated, P = phosphated, L = acid leached.

the extraframework aluminum $\{Al\}_{EF}$ present in H-USY readily reacted with phosphoric acid and formed amorphous $AlPO_4$–Al_2O_3.[15] Lischke et al. observed the formation of a crystalline $AlPO_4$ phase for a hydrothermally treated and subsequently phosphorus-modified H-ZSM-5 zeolite with the MFI topology.[17] In the work of Costa and co-workers, the zeolites H-mordenite and H-beta showed the spectroscopic signatures of $AlPO_4$ formation after phosphorus modification and hydrothermal treatment.[16] However, the authors attributed the signals to framework connected Al–O–P interactions.

Recently, we have observed the formation of an extraframework $AlPO_4$ phase in dealuminated and subsequently phosphorus-modified H-ZSM-5 with X-ray absorption microscopy.[19] It was found that the Al K-edge X-ray absorption near edge structure (XANES) spectra of the phase resembled that of tridymite. However, X-ray diffraction (XRD) patterns that could confirm this peculiar observation could not be obtained. Furthermore, although $AlPO_4$ islands were formed, it could not be elucidated whether these islands were present within the zeolite channel system or not.

In order to shed light on these fundamental questions, and to establish whether this approach is extendable to other zeolite topologies besides the 10-member ring (MR) H-ZSM-5, we have approached the phenomena of $AlPO_4$ formation in more detail by using a multipronged characterization approach. This work aims to provide a fundamental understanding of the nature of $\{Al\}_{EF}$, its reactivity toward phosphoric acid and the eventual formation of an $AlPO_4$ phase within zeolite materials. We have studied the formation of the $AlPO_4$ phase in 1-dimensional 8-, and 12-MR zeolite H-mordenite, 2-dimensional 8-, and 10-MR zeolite H-ferrierite (with FER topology) and 3-dimensional 12-MR zeolite H-USY, using a combination of scanning transmission X-ray microscopy (STXM), and ^{27}Al and ^{31}P MAS NMR spectroscopy, complemented with FT-IR spectroscopy, XRD, N_2-physisorption. Our group has recently been applying STXM in the field of zeolite chemistry and catalysis.[25−27,77] Using this experience it was possible to observe the crystallization of the extraframework $AlPO_4$ phase of H-mordenite in space and time by application of an in situ nanoreactor.[28] X-ray tomography was used to create a 3-D nanoscale chemical reconstruction of the $AlPO_4$ phase in a single H-mordenite aggregate for the first time.

EXPERIMENTAL SECTION

Sample Preparation. Details on the samples under study and related treatments are presented in Table 1 and the Supporting Information.

Ammonia Temperature-Programmed Desorption (NH_3-TPD). Ammonia TPD experiments were performed on a Micromeritics Autochem II. Samples were dried in a He flow at 600 °C for 15 min and cooled to 100 °C, after which ammonia was introduced in loops. Once the sample was saturated the temperature program was started. Under a flow of He the sample was heated with 5 °C/min to 600 °C. Outgoing NH_3 was detected by a TCD detector.

N_2-Physisorption. Isotherms were recorded using a Micromeritics Tristar 3000 setup operating at −196 °C. Prior to physisorption measurements, all samples were dried overnight at 500 °C under a N_2 flow.

Fourier Transform Infrared Spectroscopy (FT-IR). FT-IR measurements were performed on self-supporting zeolite wafers. Fifteen mg of sample was pressed with 3 tons for 10 s into a thin disk of 13 mm in diameter. The sample was evacuated to 10^{-6} bar and heated with 7 °C/min to 600 °C and immediately cooled to 150 °C. IR spectra were taken with a PerkinElmer FT-IR instrument with an optical resolution of 4 cm^{-1} and 12 accumulations with wavenumbers ranging from 4000 to 1000 cm^{-1}. Experimental details on the pyridine experiments are provided in the Supporting Information.

Scanning Transmission X-ray Microscopy (STXM). STXM experiments were performed at the Canadian Light Source (CLS) Beamline 10ID-1. Samples were dispersed in H_2O and a droplet was placed on a silicon nitride window. After drying in air the sample was placed in the STXM chamber, which was subsequently evacuated to 10^{-1} mbar. A polarized X-ray beam was obtained using a 1.6 m long, 75 mm period Apple II undulator. The X-ray beam was focused to ∼30 nm spot size on the sample plane using a Fresnel zone plate (ZP). The beam from the ZP passed through a molybdenum-based order-sorting aperture (OSA), with a 50 μm pinhole. The OSA allowed only first-order ZP diffracted light to pass. Spectral image sequences (stacks) are measured by recording images over a range of photon energies. After aligning the image sequence, spectra of the whole or a subregion were extracted for comparison. For the in situ measurements a microelectromechanical system (MEMS) designed nanoreactor was used.[28] Details on the in situ and tomography experiments are given in the Supporting Information. All STXM data analysis was performed using aXis2000.[29] Sinograms and binslices were constructed and reconstructed using the TXM-Wizard software[30] and using the iterative Algebraic Reconstruction Technique (iART) algorithm. The 3-dimensional data was analyzed using Avizo 8.0 and MATLAB.

Solid-State Nuclear Magnetic Resonance Spectroscopy (NMR). The solid-state NMR experiments were performed at 11.7 T on a Bruker Avance III 500 MHz spectrometer using a 4 mm magic

dx.doi.org/10.1021/ja508545m | J. Am. Chem. Soc. 2014, 136, 17774−17787

Table 2

type of species	description	spectroscopic signals
TFAl	Tetrahedrally coordinated framework Al and corresponding bridging hydroxyl groups	[1565 eV],[a] [55 ppm],[b] [3603 cm^{-1}][e]
OFAl	Octahedrally coordinated triple-bound framework Al physically coordinated to three H_2O molecules	[0 ppm][b]
$\{Al\}_{EF}$	Extraframework aluminum, amorphous AlO(OH)	[1568.6 eV],[a] [62 ppm, 30 ppm, 5 ppm,][b] [3650−3660 cm^{-1}][e]
$Al(PO_4)\cdot 2H_2O$	Amorphous (or semicrystalline) aluminum-phosphate	[1570.4],[a] [−12 ppm],[b] [−15 ppm, −23 ppm][c]
$AlPO_4$	Crystalline α-cristobalite/tridymite aluminum-phosphate	[1565 eV, 1571.2 eV],[a] [39 ppm],[b] [−30.5 ppm],[c] [24.8−25.1° 2θ][d]
Excess phosphates	Noninteracting ortho-, pyro-, and polyphosphates	[1.5 ppm, −6 ppm, −12 ppm][c]

[a]Al K-edge. [b]^{27}Al MAS NMR. [c]^{31}P MAS NMR. [d]XRD. [e]FT-IR.

angle spinning (MAS) probe at room temperature. The MAS rate was 15 kHz for all experiments. The ^{27}Al NMR spectra were obtained using $\pi/12$ pulses, 1000 scans and a recycling delay of 0.5 s at a rf-field of 94 kHz. The ^{31}P spectra were obtained using a pulse length of 1.8 μs, 64 scans and with a recycle delay of 60 s. The chemical shifts of ^{27}Al, and ^{31}P were externally referenced to 1 M $Al(NO_3)_{3(aq)}$, and 85% $H_3PO_{4(aq)}$, respectively.

X-ray diffraction (XRD). XRD diffractograms were obtained with a Bruker D2 X-ray powder diffractometer equipped with a Co Kα X-ray tube (λ = 1.7902 Å).

RESULTS AND DISCUSSION

Three different zeolite framework topologies have been studied in this work, i.e., MOR (mordenite), FAU (zeolite USY) and FER (ferrierite). First, we start by presenting the results of $AlPO_4$ formation in H-mordenite as measured by soft X-ray tomography and bulk-spectroscopy. The second part consists of an in situ study where the crystallization of an amorphous $AlPO_4$ phase in H-mordenite is monitored in space and time by scanning transmission X-ray microscopy (STXM). Third, we show the nature of extracted extraframework aluminum ($\{Al\}_{EF}$) and its reactivity toward phosphoric acid, and in a fourth part it is shown that lack of $\{Al\}_{EF}$ in H-mordenite prevents the formation of $AlPO_4$. We close the study on H-mordenite with an inspection of the acid site number and accessibility of the material. After that, the results on $AlPO_4$ formation in zeolite H-USY and zeolite H-ferrierite are presented. Finally, we end with a comparison of the results found for the different zeolite topologies. Previous results obtained for the MFI framework[19] (H-ZSM-5) are included in that discussion as well. On the basis of the results we will point out which different synthesis parameters should be taken into account when preparing an $AlPO_4$ phase from framework aluminum in zeolite materials. In Table 2 different species with their corresponding spectroscopic signatures are presented.

Mordenite. *Nanoscale Soft X-ray Tomography Reveals the Location of $AlPO_4$ Islands.* Sample $[MOR]_{400\text{-P-ST}}$ was prepared by applying a subsequent presteam treatment, phosphatation, and poststeam treatment to zeolite H-mordenite. More information on sample preparation and abbreviations can be found in Table 1. Using soft X-ray tomography, a set of images of the sample was collected at different photon energies during a 180° rotation. The 3-D representation of the soft X-ray absorption data is presented in Figure 1 and more information can be found in Figures S1−S3. From Figure 1 it can be observed that the single zeolite particle of sample $[MOR]_{400\text{-P-ST}}$ consists of an aggregate of smaller crystals[32] and contains specific islands that have a high concentration of phosphorus and aluminum. These islands appear to be located on the external surface of the zeolite material. Inside the aggregate, phosphorus and aluminum are also present, but in lower concentrations. The aluminum K-edge spectra that are presented in Figures 1 and S2 show the absorption white-line at 1565 eV (peak A), which is typical for AlO_4 species found in alumino-silicates.[33] The postedge feature at 1570.4 eV (peak B) is normally not observed in protonated zeolites as can be seen for the Al K-edge XANES of parent sample [MOR] in Figure S4.[34]

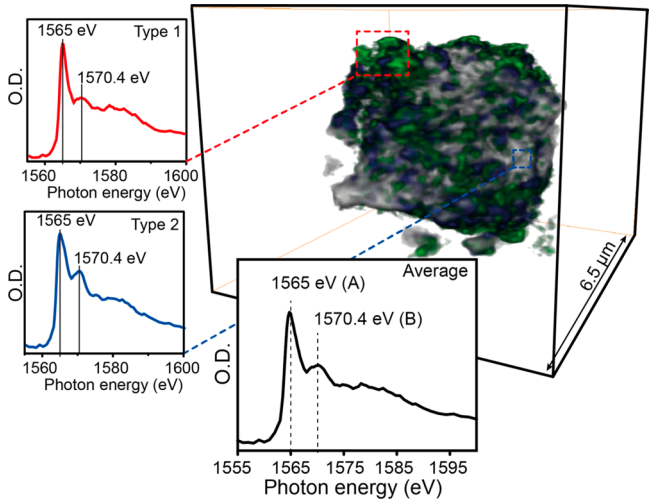

Figure 1. 3-D representation of a steamed, phosphated, and subsequently poststeamed H-mordenite aggregate, ($[MOR]_{400\text{-P-ST}}$), reconstructed from the soft X-ray tomography data. Voxel size is 63 × 63 × 63 nm^3. Gray colored voxels correspond to data collected at an energy measured before the aluminum K-edge (1555 eV) and relates to the particle density. Blue colored voxels represent the aluminum distribution and green colored voxels the phosphorus distribution. Low intensity voxels are not shown. The average Al K-edge XANES is shown in black, and was obtained by 2D STXM of the particle. It should be noted that voxels do not contain a full Al K-edge XANES. Tomography data was collected only at 1555 eV (particle density), 1565 eV (peak A) and at 1570.4 (peak B). The ratios between the recorded peak A and peak B intensities were used to identify corresponding Al phases (Type 1 and Type 2). The blue box highlights a high aluminum and high phosphorus island on the surface with corresponding Al K-edge XANES, while the red box highlights aluminum present in the crystal interior. More information on the experiment, reconstruction and XANES can be found in Figures S1−S3 and Movie S1.

The 2D STXM results shown in Figures 1 and S2, reveal that at specific regions different types of Al K-edge XANES can be found. The postedge feature at +5.5 eV from the white-line has a higher intensity in parts of the zeolite where the average aluminum and phosphorus concentration is low. This type of aluminum was indicated as Type 2 and the corresponding Al K-edge XANES is shown in Figure 1. The Type 1 aluminum

dx.doi.org/10.1021/ja508545m | J. Am. Chem. Soc. 2014, 136, 17774−17787

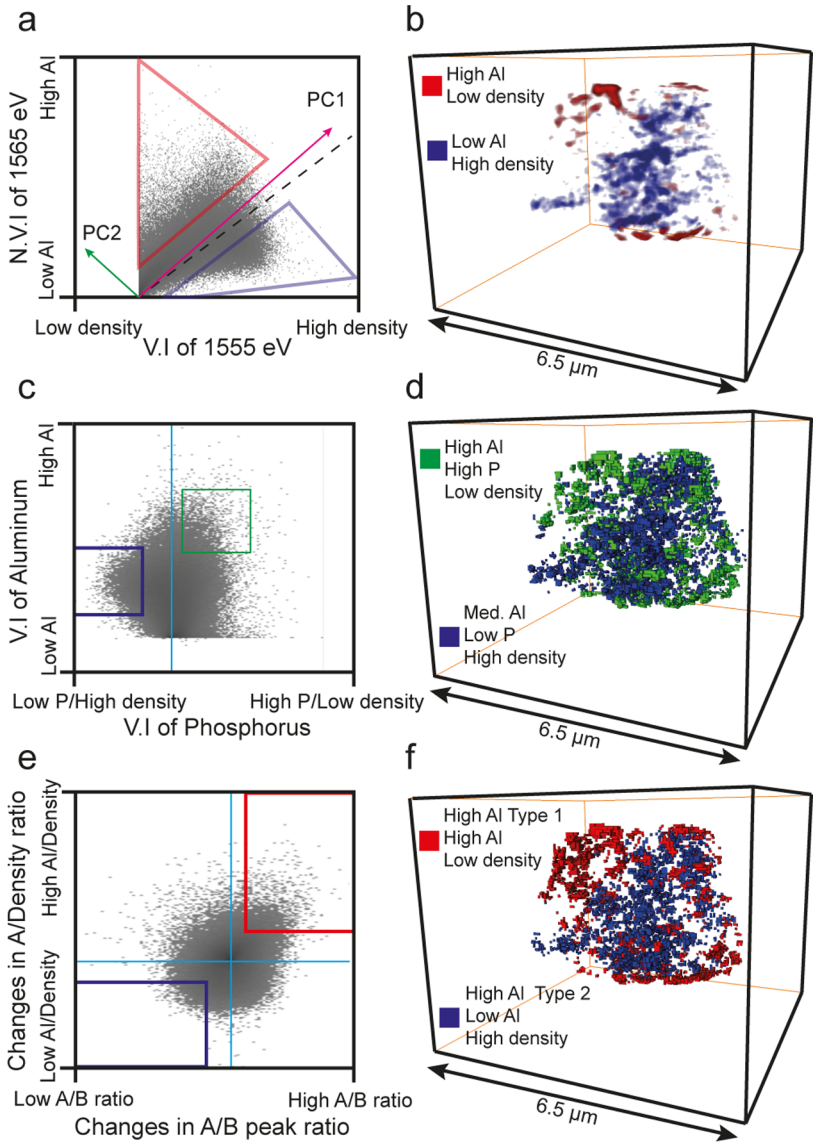

Figure 2. Statistical analysis of the particle presented in Figure 1. (a) Correlation plot of the voxel intensities (V.I) at the energy at 1555 eV (corresponding to particle density) and the normalized voxel intensities (N.V.I) at energy 1565 eV (peak A), corresponding to Al (Figure S3a,iv). The red vector indicates the positive direction of the first principle component (PC1). All voxels that lie along this line evolve in a similar manner, i.e., a linear correlation between the increase in intensity of Al and particle density. Therefore, the linear regression fit (dotted black line) has a similar slope. Any deviation from PC1 is described by the second principle component (PC2, green vector) that runs perpendicular to PC1. The red triangle indicates voxels with high Al intensity and low density, while the blue triangle indicates voxels with low Al intensity and high density. (b) 3-D representation of the voxels found along the second principle component axis that fall in the corresponding colored triangles in (a). (c) Second order correlation plot of the V.I. of phosphorus correlated with particle density (PC2 in Figure S3g) vs aluminum (PC1 in Figure S3d). The blue box indicates a region with medium aluminum intensities, high density and no or low phosphorus. The green box indicates a region with high aluminum, low density and high phosphorus intensities. (d) 3-D representation of the voxels found in the boxed regions indicated in (c). (e) Second order correlation plot of the changes in the ratio of the peaks A and B, as indicated in Figure 1 (PC2 of Figure S3d) vs the A/density ratio (PC2 of Figure 2a and S3c). High A/B ratios indicate Al Type 1, and low A/B ratios indicate Al Type 2 (Figure 1). The red box indicates a region where voxels have high aluminum, low density and high Al Type 1 intensities. The blue box indicates a region where voxels have low aluminum, high density and high Al Type 2 intensities. (f) 3-D representation of the voxels found in the boxed regions indicated in (e). More information on the construction of this figure is shown in Figure S3.

XANES, which has a low contribution of the postedge feature at +5.5 eV, is present in regions of the zeolite where the concentration of aluminum and phosphorus is high.

Statistical analysis performed on the 3-D rendered particle confirms these results. Figure 2a shows the correlation between particle density and aluminum concentration. It can be seen that aluminum is found throughout the whole aggregate. However, there is a relative decrease in Al concentration in dense parts and a higher Al concentration at lower particle densities. In Figure 2b these areas are presented in three dimensions, and it can be observed that aluminum rich zones are present as clusters on the external surface, while inside the denser parts of the crystal the concentration of aluminum is lower. The correlation plot between phosphorus, particle density and aluminum in Figure 2c,d, unequivocally show that the aluminum rich zones at the surface also contain high

dx.doi.org/10.1021/ja508545m | J. Am. Chem. Soc. 2014, 136, 17774−17787

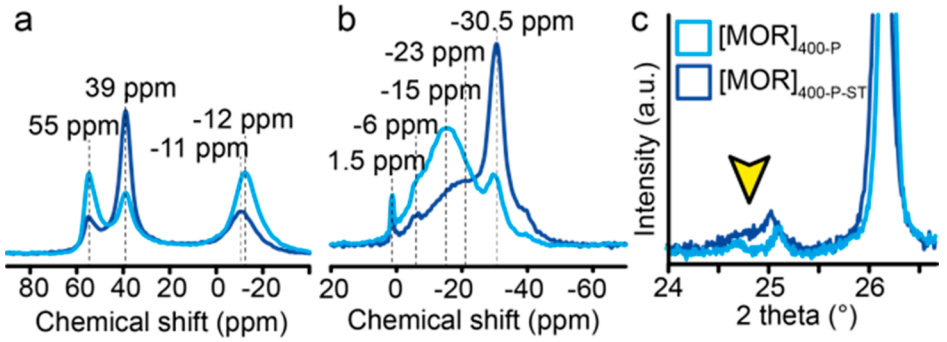

Figure 3. Sample $[MOR]_{400\text{-}P}$ (cyan) before and $[MOR]_{400\text{-}P\text{-}ST}$ (blue) after steam treatment (a) ^{27}Al MAS NMR. (b) ^{31}P MAS NMR. (c) XRD.

Scheme 1. Simplified Representation of the Concepts Proposed in This Work[a]

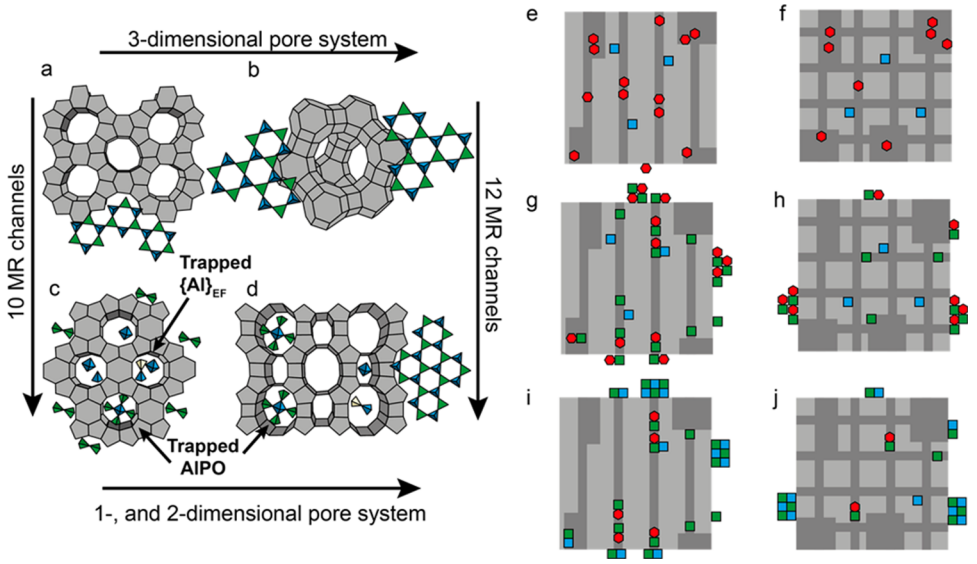

[a](a–d) Location and type of extraframework aluminum ($\{Al\}_{EF}$) species and aluminum-phosphate ($AlPO_4$) species for the framework topologies (a) MFI, (b) FAU, (c) FER, and (d) MOR. Green = phosphorus, blue = aluminum, yellow = silicon. (e–j) Different stages in the formation of $AlPO_4$ for a 1-dimensional framework (left), and a 3-dimensional framework (right). Blue = aluminum (4), red = aluminum (6), green = phosphorus. (e,f) Zeolites after hydrothermal treatment. (g,h) Formation of amorphous $AlPO_4$ phase. (i,j) crystallization of $AlPO_4$ after post-steam treatment. Frameworks are adapted from the International Zeolite Association database (MOR, FER, MFI) and from ref 31 (FAU).

concentrations of phosphorus, while dense regions of the crystals have lower aluminum and low phosphorus concentrations. Finally, Figure 2e,f shows that the Al K-edge XANES A/B peak ratio increases for aluminum found at the external surface. This indicates that Al Type 1 is more dominant in low particle density, high aluminum and high phosphorus clusters on the external surface, while Al Type 2 is more dominant in high particle density, low aluminum and low phosphorus regions deeper inside the zeolite aggregate.

The nature of the high aluminum and high phosphorus islands on the external surface was determined by inspection of the Al K-edge spectra, ^{27}Al and ^{31}P MAS NMR spectra, and X-ray diffraction. In Figure 3a the ^{27}Al MAS NMR spectra of $[MOR]_{400\text{-}P\text{-}ST}$ is presented. It can be observed that there is a sharp dominating resonance at 39 ppm. This resonance is attributed to crystalline $AlPO_4$.[17,35−38] The corresponding ^{31}P MAS NMR resonance at −30.5 ppm correlates with this assignment.[35,36] Furthermore, XRD data shows a peak around 24.8° 2θ, which only appears after a steam- or thermal treatment of sample $[MOR]_{400\text{-}P}$. This XRD peak is attributed to α-cristobalite, a berlinite polymorph.[14] Also, there is a shift to slightly lower 2θ values, indicating unit cell contraction, which follows from the removal of Al atoms from the framework.[39,40] Besides the resonance for $AlPO_4$, the ^{27}Al MAS NMR spectra of sample $[MOR]_{400\text{-}P\text{-}ST}$ shows resonances at 55 and −11 ppm. The resonance at 55 ppm is attributed to tetrahedrally coordinated framework aluminum (TFAl) species[41,42] and the −11 ppm peak to six-coordinated aluminum in amorphous AlPO, e.g., $Al(PO_4)\cdot 2H_2O$.[18] This latter assignment is in agreement with the postedge feature at +5.5 eV, found in the Al K-edge spectra of sample $[MOR]_{400\text{-}P\text{-}ST}$, as it has been attributed to six-coordinated aluminum in aluminum phosphate and can also be observed in the Al K-edge XANES of tridymite structured $AlPO_4$ and AlPO-11.[43−45]

By combining the X-ray tomography results with those from bulk spectroscopy it appears that for zeolite mordenite sample $[MOR]_{400\text{-}P\text{-}ST}$, (i) crystalline α-cristobalite/tridymite $AlPO_4$ is present on the external surface, while (ii) inside the zeolitic framework more six-coordinated aluminum in amorphous $AlPO_4$ phase is found. The latter observation is in accordance with the N_2-physisorption data in Figure S5 and Table S1. There is a decreased micropore volume of sample $[MOR]_{400\text{-}P\text{-}ST}$, compared to that of its parent sample

dx.doi.org/10.1021/ja508545m | J. Am. Chem. Soc. 2014, 136, 17774−17787

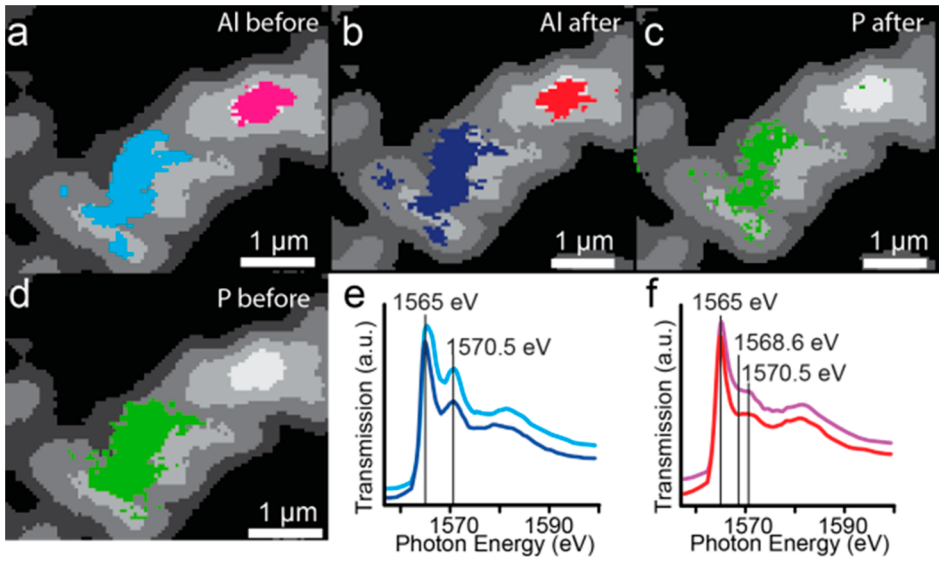

Figure 4. In situ crystallization of the aluminum-phosphate ($AlPO_4$) phase within H-mordenite monitored by scanning transmission X-ray microscopy (STXM). Chemical maps of sample $[MOR]_{400\text{-}P}$ (a,d) before and (b,c) after heating at 400 °C. Grayscale masks are constructed from the Si map and indicate the particle area. Brighter regions have a higher optical density. The colored Al K-edge XANES in (e) and (f) correspond to the colored masks in (a) and (b). (c,d) Mask of the highest phosphorus optical density. Detailed depiction of elemental distribution can be found in Figure S7.

$[MOR]_{400}$, which points to the filling of micropores. Scheme 1a and i give a simplified representation of these findings.

While parent [MOR] forms a very fine powder that is easily suspended in water, the formation of the $AlPO_4$ phase in sample $[MOR]_{400\text{-}P\text{-}ST}$ leads to the formation of millimeter-sized clusters that prove to be very hard to crush by hand. Suspension in water is extremely difficult, indicating that the hydrophobicity of the material has increased with the formation of $AlPO_4$.

In Situ STXM Shows the Crystallization of $AlPO_4$ Islands. Before the poststeam treatment, as can be observed in Figure 3a, the crystalline $AlPO_4$ phase is only present in low concentrations before hydrothermal treatment. This follows from the ^{27}Al MAS NMR spectrum of sample $[MOR]_{400\text{-}P}$ in Figure 3a, as it shows a low intensity for the 39 ppm resonance. Furthermore, the ^{27}Al MAS NMR spectrum of sample $[MOR]_{400\text{-}P}$ shows that the resonances at 55 and −12 ppm have higher intensities than after hydrothermal treatment. ^{31}P MAS NMR in Figure 3b, shows a broad resonance centered around −15 ppm and smaller resonances at −30.5, −6 and 1.5 ppm. The latter two resonances can be attributed to orthophosphate and pyrophosphate species.[46] The resonance at −15 ppm has been attributed to not fully condensed phosphates interacting with aluminum in alumina oxide hydroxide phosphate gels.[35] The smaller contribution of the resonance at −30.5 ppm, which corresponds to fully crystalline $AlPO_4$, correlates well with the smaller contribution of the ^{27}Al 39 ppm signal.[35,36]

After steam treatment there is a strong decrease in intensity of the ^{31}P −15 ppm resonance and for the ^{27}Al −12 and 55 ppm resonances. The decrease in the intensities of resonances attributed to amorphous $AlPO_4$, coincides with the increase in intensity of the resonances at ^{27}Al 39 ppm and ^{31}P −30.5 ppm. Beside the ^{31}P −30.5 ppm resonance there is also a broad resonance at ^{31}P −23 ppm after steam treatment, which are attributed to semicrystalline $AlPO_4$ domains.[35] Therefore, during steam treatment amorphous $AlPO_4$ crystallizes and forms α-cristobalite/tridymite $AlPO_4$ and semicrystalline $AlPO_4$ domains. The latter conclusion corresponds with the fact that the ^{27}Al −12 ppm resonance, corresponding to aluminum in amorphous $AlPO_4$, does not disappear completely. Furthermore, the decrease in intensity of the ^{27}Al 55 ppm resonance after steam treatment indicates that TFAl species are expelled from the framework. These species are expected to react with phosphate species to form (amorphous) $AlPO_4$.[16,47] Although we do not see the appearance of new NMR resonances and therefore no sign of $\{Al\}_{EF}$, it is possible that the resonances corresponding to these species are superimposed.

In order to see if the amorphous $AlPO_4$ phase migrates during crystallization, we performed an in situ crystallization of sample $[MOR]_{400\text{-}P}$ by heat treatment in a microelectromechanical system (MEMS) nanoreactor[28] monitored by STXM. XRD experiments showed that a heat treatment performed at 400 °C already leads to the formation of crystalline α-cristobalite as can be seen by the formation of the 24.8° 2θ peak in Figure S6.

From the X-ray absorption elemental maps shown in Figures 4 and S7 it can be observed that the $AlPO_4$ phase is already present on the outer surface of the zeolite aggregate as the concentrations of silicon and aluminum do not correlate. The corresponding Al K-edge spectra show a contribution of the +5.5 eV peak. The part of the aggregate that is low on phosphorus shows an Al K-edge XANES that has almost no contribution of the +5.5 eV peak.

After the heat treatment it can be observed that the +5.5 eV peak decreases in intensity. This effect has been described previously as the annealing of $(Al{-}O{-}P)_n$ linkages leading to the formation of α-cristobalite/tridymite $AlPO_4$.[43] It can be observed that the phase remains stationary during crystallization. A simplified representation of these results is shown in Scheme 1g and i. There is also a decrease in the postedge feature at 1568.6 eV in the Al K-edge XANES of the region that is high in aluminum content, but low in phosphorus, which is attributed to coordination changes induced by dehydration. It has been shown previously that the coordination of aluminum in H-ZSM-5, H-beta and H-mordenite change upon

dx.doi.org/10.1021/ja508545m | J. Am. Chem. Soc. 2014, 136, 17774−17787

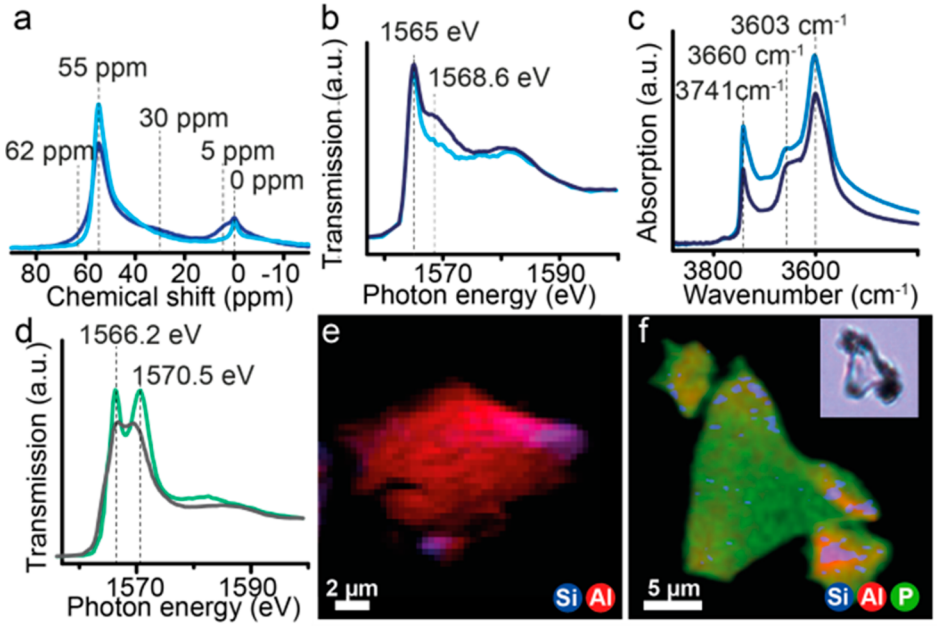

Figure 5. Microscopic and spectroscopic insights in the extraframework aluminum phase and its reaction with phosphorus acid outside zeolite H-mordenite. Samples (blue) $[MOR]_{400}$, (cyan) $[MOR]_{400\text{-L}}$. (a) ^{27}Al MAS NMR spectra. Intensities are not quantitative. (b) Al K-edge XANES. (c) FT-IR spectra. (d) Al K-edge XANES of (gray) Filtrate, (green) Filtrate + P. (e) Chemical map revealing elemental distribution in Filtrate. (f) Chemical map revealing element distribution in Filtrate + P. Inset is an optical microscopy image of the particle.

dehydration as octahedrally coordinated aluminum is reverted into four- or three-coordination.[25,48,49]

Reaction between Extraframework Aluminum Oxide Hydroxide and Phosphoric Acid. The previous results suggest that phosphoric acid reacts with aluminum in steam-treated H-mordenite to form amorphous $AlPO_4$ species. It is expected that a steam-treatment of H-mordenite leads to the formation of $\{Al\}_{EF}$. As this steam-treated zeolite is subsequently phosphated in an acidic medium, the $\{Al\}_{EF}$ species dissolve and react with phosphoric acid.[50,51] To determine which aluminum species are affected, we performed an acid leaching step where HNO_3 was used to leach out $\{Al\}_{EF}$ from the steam-treated H-mordenite sample, $[MOR]_{400}$.[40]

From Figure 5 it can be observed that before the acid leaching step, sample $[MOR]_{400}$ shows all spectroscopic signatures of a partial dealuminated material. ^{27}Al MAS NMR spectra in Figure 5a show a decrease in the resonance at 55 ppm, which indicates a decrease in TFAl atoms. There is the appearance of a broad resonance at 30 ppm, which corresponds to five-coordinated or four-coordinated $\{Al\}_{EF}$ and a resonance at 5 ppm that corresponds to six-coordinated $\{Al\}_{EF}$ species.[42,52−54] The resonance at 0 ppm is already present in the parent sample [MOR] and corresponds to framework aluminum in a six-coordinated environment due to physical coordination with water.[55,56] Furthermore, $\{Al\}_{EF}$ species can be observed as the peak at 1568.6 eV (+3.6 eV) in the Al K-edge XANES in Figure 5b[25,33] FT-IR spectroscopy shows that dealumination leads to a reduction in Brønsted acid sites as the band 3603 cm^{-1} that corresponds to bridging hydroxyl groups decreases in intensity (Figure 5c).[57] The band at 3660 cm^{-1} corresponds to Al−OH groups in $\{Al\}_{EF}$.[57] N_2-physisorption data presented in Figure S5 and Table S1 indicates a decreased pore volume, no indication of the formation of mesopores and XRD data shows that the crystalline structure of the MOR framework remains intact. Therefore, although dealumination takes place, the effects are not severe, as is expected with steam-treatment temperatures of 400 °C.

By leaching the $\{Al\}_{EF}$ species from sample $[MOR]_{400}$ with HNO_3 it can be observed from the ^{27}Al MAS NMR spectrum in Figure 5a that the resonances at 62, 30, and 5 ppm disappear. The remaining resonances are at 55 ppm, a broad tail of the 55 ppm resonance from 50 to 20 ppm, and the resonance at 0 ppm. As mentioned the 55 ppm resonance and the 0 ppm resonance stem from aluminum atoms in the framework and are not expected to be leached out by acid treatment with 0.3 M HNO_3.[40,58] We attribute the 50−20 ppm resonance to TFAl atoms in a distorted environment, i.e., partially dislodged TFAl species, which also cannot be leached out using HNO_3.[42,58]

Al K-edge XANES confirm the removal of $\{Al\}_{EF}$ species as the peak at 1568 eV disappears. Furthermore, there is an increase in the ratio between the 3603 and 3660 cm^{-1} band in the FT-IR spectra, which is in accordance with the removal of $\{Al\}_{EF}$ species.[57] One could deduce from the FT-IR spectra that sample $[MOR]_{400\text{-L}}$ contains more bridging hydroxyl groups. However, pyridine chemisorption experiments did not show an appreciable difference in the Brønsted acid site number as shown in Figure S8. Even more, in sample $[MOR]_{400}$ not all Brønsted acid sites were accessible for pyridine. Therefore, it is unlikely that bridging hydroxyl groups are retrieved by removal of extraframework cationic aluminum species, or the reinsertion of aluminum at defect sites.[59−61]

The extracted $\{Al\}_{EF}$ was characterized by XRD and STXM. The XRD patterns presented in Figure S6 show that the material is amorphous and the obtained patterns do not provide any information on the structure. However, by means of X-ray absorption microscopy we were able to determine that after extraction the $\{Al\}_{EF}$ species have an Al K-edge XANES that resembles aluminum oxide hydroxides (AlO(OH)), such as boehmite and diaspore (Figures 5d and S4).[33] Furthermore, as shown in Figure 5e, it was found that these alumina aggregates contain some silicon as well, indicating that both alumina and

dx.doi.org/10.1021/ja508545m | J. Am. Chem. Soc. 2014, 136, 17774−17787

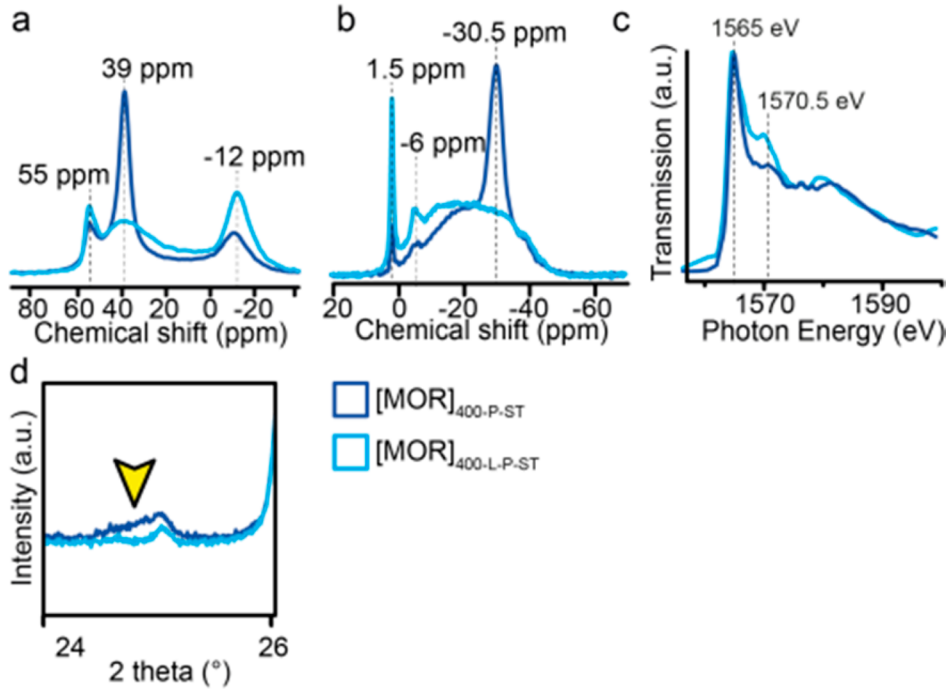

Figure 6. Samples (blue) $[MOR]_{400\text{-}P\text{-}ST}$, (cyan) $[MOR]_{400\text{-}L\text{-}P\text{-}ST}$ (a) ^{27}Al MAS NMR spectra. Intensities are not quantitative. (b) ^{31}P MAS NMR spectra. (c) Al K-edge XANES. (d) XRD.

silica are extracted from the framework. Amorphous silica−alumina has been suggested to exist as extraframework species in USY, to which an ^{27}Al MAS NMR chemical shift at 32 ppm was given.[62] However, on the basis of the low amounts of silicon observed with STXM it seems that AlO(OH) forms the majority of the leached $\{Al\}_{EF}$ species. This conclusion is in accordance with the findings of Chevreau et al., who showed that Si was present in $\{Al\}_{EF}$ of zeolite Y in concentrations lower than 5 wt %.[63]

To establish if AlO(OH) was found in the dealuminated material before acid leaching, linear regression fitting was applied to the Al K-edge XANES of sample $[MOR]_{400}$ using the Al K-edge XANES of samples MOR, $[MOR]_{400\text{-}L}$ and Filtrate as references.[25] The results of this fitting procedure are presented in Figure S9 and it can be observed that the fit correlates very well with the original spectra. We applied the same method to an H-mordenite sample that was steamed at more severe temperatures (500 °C) and found the fit to be good as well. The results indicate that $\{Al\}_{EF}$ species are present as amorphous AlO(OH) in steamed H-mordenite and not just as a product formed by acid leaching. ^{27}Al MAS NMR confirms this as the three resonances at 62, 30, and 5 ppm are also observed (at similar chemical shifts) for ground boehmite.[64] However, besides AlO(OH) it is expected that amorphous aluminum-silicate and possible other five-, and six-coordinated Al species are present as well, as silicon is detected in sample Filtrate and the Al K-edge XANES reference spectrum for AlO(OH) cannot fully reconstruct the Al K-edge XANES of [USY] (Figure S9c).

To assess what product forms after the reaction of the $\{Al\}_{EF}$ species with phosphoric acid, 0.2 g of Filtrate was reacted with 0.2 g of phosphoric acid in an aqueous solution, followed by a steam treatment. As sample Filtrate consists mainly of amorphous AlO(OH) it is expected to readily react with phosphoric acid.[14,50] It can be observed in Figure 5f and S10 that transparent tabular-shaped crystals form, which is generally the crystal habit that is described for tridymite.[65,66] From the X-ray absorption spectra in Figure 5d, it becomes apparent that the coordination of aluminum changes. There is the formation of a sharp peak at 1566.2 and 1570.5 eV. The latter peak correlates with the peak observed in the samples $[MOR]_{400\text{-}P}$ and $[MOR]_{400\text{-}P\text{-}ST}$. When the Al K-edge XANES of sample Filtrate + P is used to fit the spectra of sample $[MOR]_{400\text{-}P}$ a reasonable fit is obtained (Figure S7). As mentioned, the 1570.5 eV peak was attributed to six-coordinated aluminum in $AlPO_4$.[45] The P K-edge of sample Filtrate + P shown in Figure S4 shows that phosphorus has a 4-fold coordination.[43] The spatial distribution of phosphorus and aluminum is similar as can be seen in Figures 5f and S10.

Furthermore, it can be observed in Figure 5f and S10 that there are regions where silicon is present. In these regions, there is a high concentration of aluminum and a low concentration of phosphorus. This could indicate that there is aluminum-silicate present in the extraframework $AlPO_4$ phase and that phosphorus does not react as easily with this phase as with the AlO(OH) species. However, we did not find different Al K-edge spectra for these regions, which would suggest the concentration of a silica−alumina phase is very low, or silicon is present in a separate silica phase.

Effect of Phosphatation on Dealuminated and Acid Leached H-Mordenite. So far, the results in this work have pointed out that extraframework AlO(OH) present in dealuminated zeolite H-mordenite reacts with phosphoric acid to form extraframework amorphous $AlPO_4$ and, after thermal or hydrothermal treatment, crystallizes into α-cristobalite/tridymite $AlPO_4$. Therefore, it is expected that the removal of this $\{Al\}_{EF}$ supply prevents the formation of $AlPO_4$ after phosphorus modification. To test this hypothesis we have performed a phosphatation step followed by a poststeam treatment on acid leached sample $[MOR]_{400\text{-}L}$, which lead to the formation of sample $[MOR]_{400\text{-}L\text{-}P\text{-}ST}$.

dx.doi.org/10.1021/ja508545m | J. Am. Chem. Soc. 2014, 136, 17774−17787

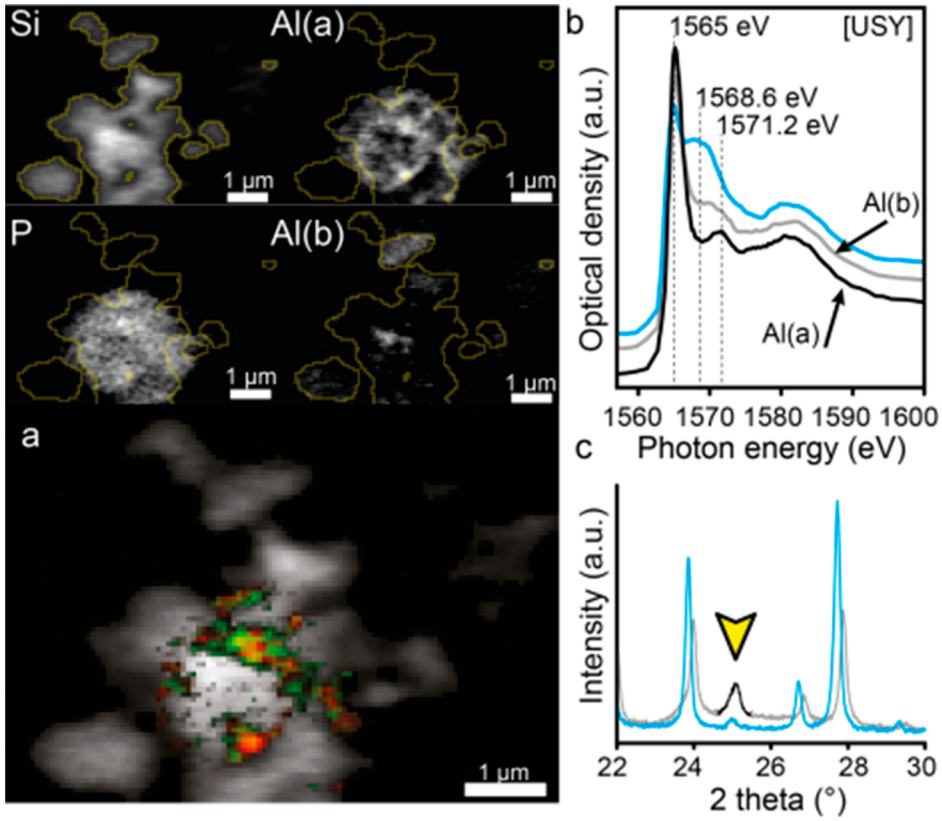

Figure 7. Scanning transmission X-ray microscopy (STXM) maps of different elements in phosphated H-USY. It can be seen that there are two types of aluminum present, i.e., Al(a), which is sited at similar positions as phosphorus and Al(b), which is located at similar positions as silicon atoms. (a) The highest optical densities found for P (green) and Al(a) (red) in respect to Si (gray). (b) Al K-edge XANES corresponding to (cyan) USY, (black) $[USY]_{P\text{-}WI\text{-}ST}$, Al(i) and (gray) $[USY]_{P\text{-}WI\text{-}ST}$, Al(ii). STXM results from another aggregate of sample $[USY]_{P\text{-}WI\text{-}ST}$ are presented in Figure S14. (c) XRD data of sample (cyan) USY, (gray) $[USY]_{P\text{-}WI\text{-}ST}$.

As expected, the structural characterization results presented in Figure 6 show that there is no indication of the formation of crystalline $AlPO_4$ in sample $[MOR]_{400\text{-}L\text{-}P\text{-}ST}$, as the ^{27}Al MAS NMR resonance at 39 ppm, the ^{31}P MAS NMR resonance at −30.5 ppm, the Al K-edge XANES postedge feature at +5.5 eV and the XRD 24.8° 2θ peak are not observed. However, phosphatation still influences the remaining aluminum species, as there is a change in the ^{27}Al MAS NMR spectra in comparison to that of sample $[MOR]_{400\text{-}L}$ presented in Figure 5a. There is a strong decrease in the 55 ppm peak and there is the formation of a broad band around 40 ppm. The most intense resonance of the ^{27}Al MAS NMR spectrum of $[MOR]_{400\text{-}L\text{-}P\text{-}ST}$ is at −12 ppm, which we attributed to amorphous $AlPO_4$. However, the expected corresponding ^{31}P MAS NMR resonance at −15 ppm is not observed. Also, the Al K-edge spectrum of sample $[MOR]_{400\text{-}P\text{-}ST}$ does not show the postedge feature at 1570.5 eV and there is no strong correlation in the location of phosphorus and aluminum atoms as shown in Figure S11.

However, when linear regression fitting is applied using the Al K-edge XANES of Filtrate + P as a reference, it can be observed that there are regions in the sample that have a better correlation with phosphorus position and also show an Al K-edge spectra that resembles that of Filtrate + P (Figure S11). Therefore, it cannot be ruled out that phosphorus does form extraframework $AlPO_4$ species. It is expected that the formation of $\{Al\}_{EF}$ and subsequent reaction with phosphate species during the poststeam treatment induces the formation of amorphous or crystalline AlPO.[16] Also, since phosphoric acid is a complexing acid, it is possible that it can remove partially dislodged aluminum species from the framework which HNO_3 cannot.[40]

Acidity in Dealuminated and Phosphated Materials. Ammonia temperature-programmed desorption of sample $[MOR]_{400\text{-}P\text{-}ST}$ shows a 85% decrease in ammonia desorbed at temperatures above 300 °C as can be seen in Figure S8. A similar decrease in the number of strong acid sites in comparison to parent sample MOR is therefore expected. Sample $[MOR]_{400\text{-}P\text{-}ST}$ has two desorption maxima, at 175 and 425 °C (Figure S8). The low temperature desorption maximum corresponds to weak acid sites that are not observed in the parent sample, while the high desorption maximum corresponds to strong acid sites. FT-IR infrared is in accordance with the observation of strong acid sites, as there is still a band present at 3603 cm^{-1} that corresponds to bridging hydroxyl groups, shown in Figure S8 and S12. However, the accessibility of these acid sites is limited for pyridine, as the FT-IR spectrum in Figure S8 does not show the formation protonated pyridinium ions and the bridging hydroxyl groups are not affected. Furthermore, it can be observed that this effect is observed for all phosphated samples, indicating that a 4 wt % loading of phosphorus effectively blocks the 1-dimensional pore system of the mordenite framework.

Extension of the Phosphatation Method to Other Zeolite Framework Topologies. *Faujasite.* As zeolite H-USY with FAU topology already contains an $\{Al\}_{EF}$ supply, it was not necessary to apply a presteam treatment.[15] When the H-USY sample was treated with phosphoric acid and HNO_3

dx.doi.org/10.1021/ja508545m | J. Am. Chem. Soc. 2014, 136, 17774−17787

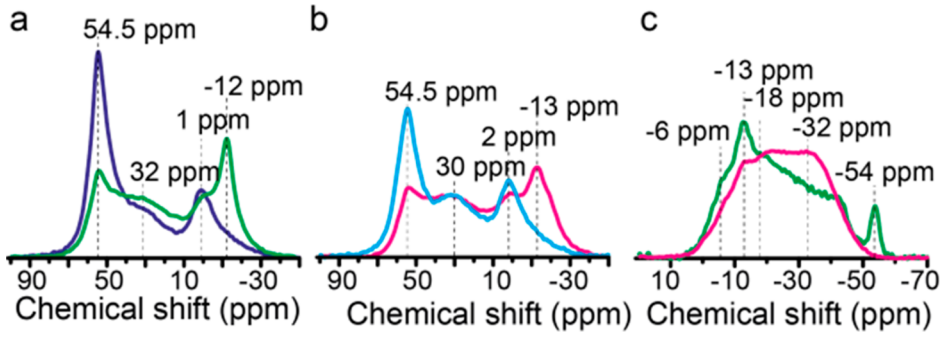

Figure 8. (a) ^{27}Al MAS NMR of sample (blue) $[FER]_{500}$, (green) $[FER]_{500\text{-}P\text{-}ST}$. (b) ^{27}Al MAS NMR of sample (cyan) $[FER]_{600}$, (magenta) $[FER]_{600\text{-}P\text{-}ST}$. (c) ^{31}P MAS NMR of sample (green) $[FER]_{500\text{-}P\text{-}ST}$, (magenta) $[FER]_{600\text{-}P\text{-}ST}$.

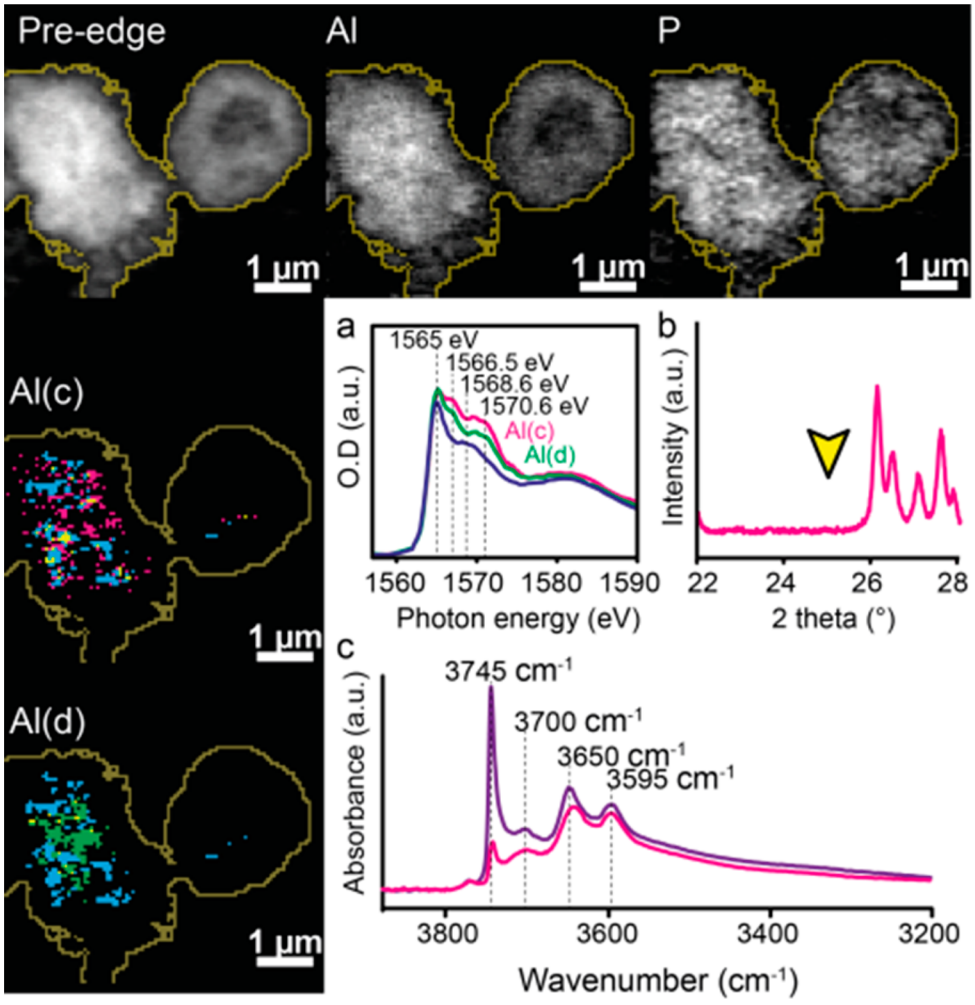

Figure 9. Scanning transmission X-ray microscopy (STXM) maps of different elements in phosphated FER ST 500. Scale bar is 1 μm. Using a linear regression fitting, Al(c) and Al(d) can be distinguished. It can be observed that the distribution of high concentrations of P (cyan) and Al(d) (green) hardly overlap (yellow). There is slightly more overlap (yellow) between P (cyan) and Al(c) (magenta); however, there is no clear correlation. (a) Corresponding Al K-edge XANES of (blue) $[FER]_{500}$, (green) $[FER]_{500\text{-}P\text{-}ST}$ Al(i), and (magenta) $[FER]_{500\text{-}P\text{-}ST}$ Al(ii). (b) XRD data of sample $[FER]_{600\text{-}P\text{-}ST}$. (c) FT-IR data of (purple) $[FER]_{600}$, and (magenta) $[FER]_{600\text{-}P\text{-}ST}$.

under reflux conditions, XRD data presented in Figure S13 showed that the material became amorphous. It is assumed that the use of additional HNO_3 caused the collapse of the framework structure and an amorphization of the material.[67] An acid treatment without phosphoric acid leads to severe amorphization as well (Figure S13). Interestingly, the XRD patterns of sample $[USY]_{P\text{-}ST}$, which are presented in Figure S13, do not show the formation of crystalline $AlPO_4$. Therefore, it appears that the amorphous alumino-silicate phase that is expected to form after the framework collapse, does not react with phosphoric acid. This is supported by the results of Filtrate + P shown in Figure 5f where regions of silicon and aluminum was found in the sample, but not phosphorus.

In order to prevent excessive leaching of framework aluminum, the phosphatation was performed by wet impregnation with an aqueous solution containing only H_3PO_4. The

dx.doi.org/10.1021/ja508545m | J. Am. Chem. Soc. 2014, 136, 17774−17787

phosphorus P/Al ratio was decreased from 1 to 0.5. This approach was effective, as it did not lead to total framework collapse as can be observed from the XRD diffractogram in Figure 7c. STXM and X-ray diffraction results clearly show the formation of an extraframework $AlPO_4$ phase. As can be seen in Figure 7, the presented $[USY]_{P\text{-}WI\text{-}ST}$ aggregate shows a large concentration of aluminum and phosphorus that is located around the central part of the aggregate. The Al K-edge XANES Al(a), which corresponds to this $AlPO_4$ cluster is significantly different from the Al K-edge XANES Al(b), found in the zeolitic silicon rich regions. Spectra Al(a) resembles that of crystalline $AlPO_4$ as has been previously observed for the sample $[MOR]_{400\text{-}P\text{-}ST}$ and tridymite in $AlPO_4$ thin-films.[43] The crystallinity of the $AlPO_4$ is even higher for the sample $[USY]_{P\text{-}WI\text{-}ST}$ than for sample $[MOR]_{400\text{-}P\text{-}ST}$ as can be seen by the distinct postedge feature at 1571.2 eV. The large crystalline $AlPO_4$ clusters are confirmed by the sharp XRD peak around 25.1°, which corresponds to α-cristobalite.[14] The crystallite sizes range between 30 to 40 nm, as determined by the Scherrer equation. The large crystal sizes and the clearly observable $AlPO_4$ phase with STXM can in part be attributed to the fact that H-USY has a much larger aluminum supply, due to its low Si/Al ratio of 2.55, in comparison to H-mordenite.

These results are in full accordance with the study performed by Corma and co-workers.[15] It was found that phosphoric acid readily reacts with the $\{Al\}_{EF}$ species in zeolite H-USY to form an amorphous $AlPO_4$ phase. After steam treatment it was found that the phase crystallizes into $AlPO_4$. The authors suggested that the phase was tridymite, and on the basis of N_2 physisorption data, it was postulated that the phase could be found on the external surface of the zeolite. Using X-ray absorption microscopy and X-ray diffraction there is now direct prove for these suggestions.

Ferrierite. From the previous results would appear that an extraframework $AlPO_4$ phase can be created from a zeolite's own supply by simply applying a dealumination step followed by a phosphatation step. However, the results obtained for phosphated zeolite H-ferrierite show that this assumption is not necessarily correct. As can be observed in Figure 8, the ^{27}Al MAS NMR and ^{31}P MAS NMR spectra show no indication on the formation of crystalline $AlPO_4$, as a sharp and intense resonance at 39 ppm would be expected in the ^{27}Al MAS NMR spectra and one at −28 or −31 ppm for the ^{31}P MAS NMR.[15,16,18,19]

However, in contrast to acid-leached H-mordenite, the lack of the $AlPO_4$ cannot be attributed to the absence of an $\{Al\}_{EF}$ phase. From Figure 8 it can be observed that H-ferrierite steamed at 500 °C, shows a strong contribution of the ^{27}Al MAS NMR resonance at 32 ppm, corresponding to $\{Al\}_{EF}$ species.[19,68,69] The resonance at 30 ppm is even more pronounced for H-ferrierite steamed at 600 °C. Furthermore, in Figure 9, the Al K-edge XANES of steamed H-ferrierite shows a peak at 1568.6 eV, corresponding to $\{Al\}_{EF}$ species and the FT-IR band of steamed H-ferrierite at 3650 cm^{-1} corresponds to Al−OH species in $\{Al\}_{EF}$.[25,33,69] Therefore, the presence of $\{Al\}_{EF}$ species can be confirmed. It is reported in the literature that leaching out $\{Al\}_{EF}$ from zeolite H-ferrierite after steam treatment is very difficult.[68,69] It has been suggested that $\{Al\}_{EF}$ species in H-ferrierite are trapped in the structure as migration of aluminum to the surface has not been observed, while at the same time $\{Al\}_{EF}$ species were detected, which could not be washed out.[68] Although the exact origins of the trapped $\{Al\}_{EF}$ species is not well understood, one of the suggestions was that this type of $\{Al\}_{EF}$ was trapped in the 8-ring channels and resistant to acid washing.[68]

The inaccessible nature of these $\{Al\}_{EF}$ species follows from our results as well. First, it can be observed that the ^{27}Al MAS NMR resonances at 32 and 0 ppm remain almost unaffected after phosphatation. The only observable change is a decrease in intensity of the 54.5 ppm resonance and the appearance of a new resonance at −12 ppm, which would indicate that the latter forms at the cost of the former. Second, the FT-IR spectra shown in Figure 9c show that while the intensity of the band for external Si−OH groups at 3745 cm^{-1} decreases sharply, the intensity of the band at 3650 cm^{-1}, corresponding to Al−OH groups, is not affected. In contrast, we have shown that the intensity of the bands corresponding to terminal Al−OH groups decrease significantly after the phosphatation of H-ZSM-5.[19,58] From the X-ray absorption maps in Figure 9 it follows that location of phosphorus and aluminum does not correlate, which further indicates that most phosphorus does not interact with aluminum in zeolite H-ferrierite. A schematic representation of this effect is shown in Scheme 1c.

Finally, the Al K-edge XANES presented in Figure 9 do not show a decrease in the 1568.6 eV peak as was observed for sample $[MOR]_{400\text{-}P}$ for steamed H-ZSM-5.[19] However, there is a new spectrum that contributes to the overall XANES as two peaks at 1566.5 and 1570.6 eV appear. These values correspond to those of Filtrate + P. Linear regression fitting of the $[FER]_{500\text{-}P\text{-}ST}$ XANES, shown in Figure S15, using the Al K-edge XANES of Filtrate + P as a reference indicate the latter spectrum has a contribution to the overall spectrum.

Influence of Zeolite Topology on $AlPO_4$ Formation. From the results described in the previous sections and from the results recently obtained in our study on H-ZSM-5,[19] we are now in the position to discuss some of the parameters that should be taken into account in the synthesis of $AlPO_4$ from the framework aluminum of zeolite materials. The most important factor is the availability of reactive aluminum. A steam treatment is an effective route to obtain reactive aluminum, since during steam treatment aluminum is expelled from the framework and forms dominantly extraframework AlO(OH), as shown in Scheme 1e,f. These species are very reactive toward H_3PO_4 and form amorphous AlPO.[15,17,19] However, aluminum that is still connected to the zeolitic framework is not be able to form $AlPO_4$, as long as there are still framework Si−O−Al bonds left, as can be observed in Scheme 1g,h.[19,58] We also expect $AlPO_4$ not to form by reaction of amorphous silica−alumina with phosphoric acid.[70] Therefore, the tendency of framework aluminum to be hydrolyzed during steaming conditions is an important factor that determines if reactive aluminum is formed or not. Unfortunately, to our best knowledge, not many studies on the exact effect of framework topology on hydrothermal stability have been reported in the literature. In the works of Costa and Caeiro et al. it is reported that identical hydrothermal treatments on zeolites with comparable Si/Al ratios, lead to an 80% loss of TFAl atoms in H-mordenite, 60% loss in H-ZSM-5, and 15% in H-beta.[16,71] Therefore, it is clear that the hydrothermal stability of framework aluminum is different for different zeolite topologies. If formed $\{Al\}_{EF}$ species are trapped in the framework, as for H-ferrierite, they are inaccessible to phosphoric acid and $AlPO_4$ will not form.[68,69]

Depending on the framework type, framework aluminum and partially dislodged framework aluminum can also be

dissolved by mineral acids and extracted from the framework, allowing these species to react with phosphoric acid. It has been shown that dissolution of framework aluminum is possible in framework structures such as H-mordenite and aluminum rich H-USY,[51,63,67] but more difficult in materials such as zeolite H-beta,[72] H-ZSM-5,[73] and H-ferrierite.[74] Therefore, even for a mildly steamed sample, such as H-mordenite, most of the aluminum present in the zeolite is extracted from the framework and high amount of crystalline $AlPO_4$ will be formed, as was shown in this work. For H-ZSM-5 we did observe the formation of an $AlPO_4$ phase, although the amount was lower than for H-mordenite, as a consequence the XRD patterns of the former sample did not show a peak for α-cristobalite.[19] However, the P/Al ratio used in that study was 0.5 instead of P/Al = 1 which is used in the current study and no additional HNO_3 was added. Therefore, the phosphorus content and acidity of the solution used in phosphatation is also a factor that should be considered.

This follows from the results on H-USY from this study, which show that if the framework Si/Al ratio is very low (Si/Al bulk ratio = 2.55), the extraction of framework aluminum will destabilize the framework and lead to a collapse of the structure. When HNO_3 was left out of the phosphatation step and the P/Al ratio was decreased to 0.5, the framework structure was better preserved and crystalline $AlPO_4$ was formed.

It has been reported that oxalic acid, being a complexing agent, is more effective in dissolving framework aluminum from zeolites H-mordenite and H-beta than mineral acids.[40,75] Therefore, it is possible that phosphoric acid, which is also a chelating agent for aluminum cations, is capable of extracting more framework aluminum from the zeolite than HNO_3.

During thermal or hydrothermal treatment of the amorphous $AlPO_4$ phase $(Al-O-P)_n$ linkages anneal, which leads to the crystallization of the amorphous $AlPO_4$ phase as shown in Scheme 1i,j. In order for the $AlPO_4$ phase to grow as 3-dimensional crystal structures, sufficient space is needed. Therefore, it is assumed that if $AlPO_4$ is located inside the zeolite micropores crystallization is inhibited, leading to the higher concentration of amorphous $AlPO_4$ found inside the zeolite H-mordenite. Such an effect was not observed for zeolite H-USY, as for the samples under study the $AlPO_4$ phase was found exclusively outside of the crystal. Al K-edge XANES of silicon rich parts showed a spectrum that resembled four-coordinated aluminum in aluminum-silicates, as can be seen in Figure 7 and S14.[33] The results reported by Corma and co-workers are in accordance with this observation, as they showed by ^{27}Al MAS NMR that the −12 ppm resonance for amorphous $AlPO_4$ was almost eliminated after the crystallization of the $AlPO_4$ phase in H-USY.[15] For dealuminated, phosphated and poststeamed H-ZSM-5, we observed a decrease in mesopore volume after phosphorus introduction, which could indicate the presence $AlPO_4$ in the interior parts of zeolite H-ZSM-5.[19] However, there are no indications that the $AlPO_4$ phase was more amorphous. It is postulated that the pore dimensionality of the framework plays a role. The 1-dimensional pore structure of zeolite H-mordenite is prone to pore-blockage (Scheme 1i), leading to the parts of the $AlPO_4$ phase to be trapped inside the channel system, hindering subsequent crystallization. In the 3-dimensional channel system of zeolite H−Y and H-ZSM-5, these constrains are not as dominant and there will be a stronger segregation between (i) $AlPO_4$ outside the zeolite and (ii) framework aluminum inside the zeolite (Scheme 1j). However, further studies will be necessary to fully substantiate these claims.

Besides crystallization of the $AlPO_4$ phase, the poststeam treatment also leads to further dealumination. The formed $\{Al\}_{EF}$ species are expected to react with phosphate species to form additional $AlPO_4$, as could be observed for zeolite H-mordenite and presented in Scheme 1i,j. Costa and co-workers showed that the addition of phosphates to fresh and unmodified zeolite H-beta and H-mordenite, followed by a steam treatment (800 °C, 5 h) converted the majority of the framework aluminum into crystalline extraframework $AlPO_4$. Also, Zhuang et al. obtained similar results for phosphated H-ZSM-5 after a steam treatment (800 °C, 10 h). It is interesting how this relates to the well-known promotional effect of phosphorus on the hydrothermal stability H-ZSM-5, but beyond the scope of this work.[17,71,76]

In the case of H-ferrierite, due to the inaccessible nature of the $\{Al\}_{EF}$ species, the formation of a crystalline $AlPO_4$ phase is unlikely to take place. However, we suggest that the applied poststeam treatment leads to further dealumination, as expelled aluminum species will react with the phosphates that are present in the channel system, to form amorphous $AlPO_4$. The spectroscopic signals found at −12 ppm in ^{27}Al MAS NMR spectroscopy and 1566.5 and 1570.6 eV in Al K-edge XANES microscopy support this hypothesis. We further postulate that these $AlPO_4$ species become trapped in the framework similar to the $\{Al\}_{EF}$ species, as N_2 -physisorption data in Figure S5 Table S1 shows that the pore volume decreases further after poststeam treatment.

As this is, to our best knowledge, one of the few works that explores the creation of a zeolite binder material made from components of the zeolite itself, it is too premature to present a fully unified view on $AlPO_4$ formation in zeolite materials. However, we do hope that this work may stimulate future characterization studies that further explore these promising avenues.

CONCLUSIONS

A detailed study has been performed on the formation of an aluminum-phosphate ($AlPO_4$) binder from the framework aluminum supply of three industrially relevant zeolites; H-USY, H-mordenite and H-ferrierite. It has been found that the dealumination of the zeolite materials by hydrothermal treatment has an extraframework aluminum ($\{Al\}_{EF}$) phase, with amorphous AlO(OH) phase as the main component. The presence of small traces of silicon implied that amorphous silica−alumina was also present in the $\{Al\}_{EF}$ phase. When the dealuminated zeolite sample was suspended in an acidic aqueous solution containing phosphoric acid, the AlO(OH) species readily reacted with phosphoric acid and an amorphous extraframework $AlPO_4$ phase was formed. If the $\{Al\}_{EF}$ species were trapped in the framework, as was the case for zeolite H-ferrierite, they remained inaccessible to phosphoric acid and an $AlPO_4$ phase could not form. Extraframework amorphous silica−alumina and framework-connected aluminum were not found to participate in the formation of $AlPO_4$. However, acid leaching of framework aluminum was observed in H-USY, leading to a collapse of the framework and severe amorphization.

The amorphous $AlPO_4$ phase was found to consist of four- and six-coordinated aluminum connected to PO_4^- units. Silicon was found in the $AlPO_4$ phase as well, although indications for an interaction with phosphorus or $AlPO_4$ have not been

dx.doi.org/10.1021/ja508545m | J. Am. Chem. Soc. 2014, 136, 17774−17787

observed. The amorphous $AlPO_4$ phase was found to be heterogeneously distributed on the external zeolitic surface. Although the phase was found to be located in the zeolitic interior as well, this was at lower concentrations. It is suggested that the $AlPO_4$ phase is more likely to become trapped in an 1-dimensional channel system, than in a 3-dimensional channel system.

During a subsequent thermal or hydrothermal treatment the amorphous $AlPO_4$ phase crystallizes into $AlPO_4$ with an α-cristobalite/tridymite structure. The phase was not observed to migrate during crystallization. The crystalline α-cristobalite/tridymite $AlPO_4$ forms islands, which are located at the external surface of the zeolite materials. The $AlPO_4$ phase that was present in the crystal interior was found to consist of more aluminum atoms with a 6-fold coordination. It was suggested that $AlPO_4$ located in the zeolite channel system has the tendency to remain more amorphous due to spatial constraints inhibiting crystallization. Besides crystallization of the $AlPO_4$ phase, a poststeam treatment leads to progressed dealumination of the zeolite material. The $\{Al\}_{EF}$ that is formed subsequently reacts with phosphate species to form additional (amorphous) $AlPO_4$. After the crystalline $AlPO_4$ phase was formed in H-mordenite, the samples form millimeter-sized clusters with an increased hydrophobicity.

■ ASSOCIATED CONTENT

Supporting Information

Sample map, tomography information, Al K-edge XANES, FT-IR spectra, extended ^{27}Al MAS NMR spectra, ^{31}P MAS NMR spectra, XRD diffractograms, N_2-physisorption data, ammonia TPD and pyridine adsorption, STXM elemental maps and fit results. A movie of the 3-D reconstructed particle is presented as well. This material is available free of charge via the Internet at http://pubs.acs.org.

■ AUTHOR INFORMATION

Corresponding Author

b.m.weckhuysen@uu.nl

Notes

The authors declare no competing financial interest.

■ ACKNOWLEDGMENTS

The authors would like to thank beamline 10ID-1 (SM) at the Canadian Light Source (CLS) for beamtime and support. CLS is supported by the Natural Sciences and Engineering Research Council of Canada, the National Research Council Canada, the Canadian Institutes of Health Research, the Province of Saskatchewan, Western Economic Diversification Canada, and the University of Saskatchewan. Furthermore, Joris Goetze, Mustafa Al Samarai and Ramon Oord of Utrecht University are kindly thanked for their help during the STXM measurements. Prof. Dr. Henny Zandbergen and Dr. Meng-Yue Wu from TU Delft are thanked for supplying a MEMS in situ nanoreactor. N_2-physisorption measurements were performed at Utrecht University by Arjan den Otter, Nazila Masoud and Dr. Ying Wei.

■ REFERENCES

(1) Vermeiren, W.; Gilson, J. P. *Top. Catal.* **2009**, *52*, 1131.
(2) Otterstedt, J. E.; Gevert, S. B.; Jåås, S. G.; Menon, P. G. *Appl. Catal.* **1986**, *22*, 159.
(3) Mohanty, S.; Kunzru, D.; Saraf, D. *Fuel* **1990**, *69*, 1467.
(4) Guisnet, M.; Gilson, J.-P. *Zeolites for Cleaner Technologies*; Imperial College Press: London, 2002; Vol. 3.
(5) Olsbye, U.; Svelle, S.; Bjørgen, M.; Beato, P.; Janssens, T. V. W.; Joensen, F.; Bordiga, S.; Lillerud, K. P. *Angew. Chem., Int. Ed.* **2012**, *51*, 5810.
(6) Caro, J.; Noack, M.; Kölsch, P. *Adsorption* **2005**, *11*, 215.
(7) Jae, J.; Coolman, R.; Mountziaris, T. J.; Huber, G. W. *Chem. Eng. Sci.* **2014**, *108*, 33.
(8) Mitchell, S.; Michels, N.-L.; Perez-Ramirez, J. *Chem. Soc. Rev.* **2013**, *42*, 6094.
(9) Hargreaves, J. S. J.; Munnoch, A. L. *Catal. Sci. Technol.* **2013**, *3*, 1165.
(10) Cao, G.; Martens, L. R. M.; White, J. L.; Chen, T. J.; Shah, M. J. US6080303 A, June 27, 2000.
(11) Corma, A. WO1999002260 A1, January 21, 1999.
(12) Kirker, G. W.; Landis, M. E.; Yen, J. H. US4724066 A, February 9, 1988.
(13) Roberie, T. G.; John, F. T. I. I. US5286369 A, February 15, 1994.
(14) Lee, Y.-J.; Kim, Y.-W.; Viswanadham, N.; Jun, K.-W.; Bae, J. W. *Appl. Catal., A* **2010**, *374*, 18.
(15) Corma, A.; Fornes, V.; Kolodziejski, W.; Martineztriguero, L. J. *J. Catal.* **1994**, *145*, 27.
(16) Costa, A. F.; Cerqueira, H. S.; Ferreira, J. M. M.; Ruiz, N. M. S.; Menezes, S. M. C. *Appl. Catal., A* **2007**, *319*, 137.
(17) Lischke, G.; Eckelt, R.; Jerschkewitz, H. G.; Parlitz, B.; Schreier, E.; Storek, W.; Zibrowius, B.; Öhlmann, G. *J. Catal.* **1991**, *132*, 229.
(18) Zhuang, J.; Ma, D.; Yang, G.; Yan, Z.; Liu, X.; Liu, X.; Han, X.; Bao, X.; Xie, P.; Liu, Z. *J. Catal.* **2004**, *228*, 234.
(19) van der Bij, H. E.; Aramburo, L. R.; Arstad, B.; Dynes, J. J.; Wang, J.; Weckhuysen, B. M. *ChemPhysChem* **2014**, *15*, 283.
(20) Majano, G.; Delmotte, L.; Valtchev, V.; Mintova, S. *Chem. Mater.* **2009**, *21*, 4184.
(21) Machado, F. J.; López, C. M.; Centeno, M. A. A.; Urbina, C. *Appl. Catal., A* **1999**, *181*, 29.
(22) Hartmann, M. *Angew. Chem., Int. Ed.* **2004**, *43*, 5880.
(23) Perez-Ramirez, J.; Christensen, C. H.; Egeblad, K.; Christensen, C. H.; Groen, J. C. *Chem. Soc. Rev.* **2008**, *37*, 2530.
(24) Janardhan, H. L.; Shanbhag, G. V.; Halgeri, A. B. *Appl. Catal., A* **2014**, *471*, 12.
(25) Aramburo, L. R.; de Smit, E.; Arstad, B.; van Schooneveld, M. M.; Sommer, L.; Juhin, A.; Yokosawa, T.; Zandbergen, H. W.; Olsbye, U.; de Groot, F. M. F.; Weckhuysen, B. M. *Angew. Chem., Int. Ed.* **2012**, *51*, 3616.
(26) Aramburo, L. R.; Liu, Y.; Tyliszczak, T.; de Groot, F. M. F.; Andrews, J. C.; Weckhuysen, B. M. *ChemPhysChem* **2013**, *14*, 496.
(27) de Groot, F. M. F.; de Smit, E.; van Schooneveld, M. M.; Aramburo, L. R.; Weckhuysen, B. M. *ChemPhysChem* **2010**, *11*, 951.
(28) Creemer, J.; Helveg, S.; Hoveling, G.; Ullmann, S.; Molenbroek, A.; Sarro, P.; Zandbergen, H. *Ultramicroscopy* **2008**, *108*, 993.
(29) Hitchcock, A. P. *aXis2000*; McMaster University: Hamilton, Ontario, 2008; http://unicorn.mcmaster.ca/aXis2000.html (accessed July 26, 2014). aXis2000 is written in Interactive Data Language (IDL).
(30) Liu, Y.; Meirer, F.; Williams, P. A.; Wang, J.; Andrews, J. C.; Pianetta, P. *J. Synchrotron Radiat.* **2012**, *19*, 281.
(31) Boddenberg, B.; Rakhmatkariev, G. U.; Hufnagel, S.; Salimov, Z. *Phys. Chem. Chem. Phys.* **2002**, *4*, 4172.
(32) van Laak, A. N. C.; Sagala, S. L.; Zečević, J.; Friedrich, H.; de Jongh, P. E.; de Jong, K. P. *J. Catal.* **2010**, *276*, 170.
(33) Ildefonse, P.; Cabaret, D.; Sainctavit, P.; Calas, G.; Flank, A. M.; Lagarde, P. *Phys. Chem. Miner.* **1998**, *25*, 112.
(34) Shimizu, K.-i.; Kato, Y.; Yoshida, H.; Satsuma, A.; Hattori, T.; Yoshida, T. *Chem. Commun.* **1999**, 1681.
(35) Huang, Y.; Richer, R.; Kirby, C. W. *J. Phys. Chem. B* **2003**, *107*, 1326.
(36) Blackwell, C. S.; Patton, R. L. *J. Phys. Chem.* **1984**, *88*, 6135.
(37) Liu, G.; Jia, M.; Zhou, Z.; Zhang, W.; Wu, T.; Jiang, D. *Chem. Commun.* **2004**, 1660.

(38) Sanz, J.; Campelo, J. M.; Marinas, J. M. *J. Catal.* **1991**, *130*, 642.
(39) Reddy, K.; Song, C. *Catal. Lett.* **1996**, *36*, 103.
(40) Giudici, R.; Kouwenhoven, H. W.; Prins, R. *Appl. Catal., A* **2000**, *203*, 101.
(41) Klinowski, J. *Prog. Nucl. Magn. Reson. Spectrosc.* **1984**, *16*, 237.
(42) Chen, T.-H.; Wouters, B. H.; Grobet, P. J. *Eur. J. Inorg. Chem.* **2000**, *2000*, 281.
(43) Daviero, S.; Ibanez, A.; Avinens, C.; Flank, A.; Philippot, E. *Thin Solid Films* **1993**, *226*, 207.
(44) Fröba, M.; Tiemann, M. *Chem. Mater.* **1998**, *10*, 3475.
(45) Aoki, Y.; Hirata, S.; Habazaki, H. *J. Electrochem. Soc.* **2011**, *158*, P41.
(46) Caro, J.; Bülow, M.; Derewinski, M.; Haber, J.; Hunger, M.; Kärger, J.; Pfeifer, H.; Storek, W.; Zibrowius, B. *J. Catal.* **1990**, *124*, 367.
(47) Cardoso, M. J. B.; Rosas, D. D. O.; Lau, L. Y. *Adsorption* **2005**, *11*, 577.
(48) Omegna, A.; Prins, R.; van Bokhoven, J. A. *J. Phys. Chem. B* **2005**, *109*, 9280.
(49) van Bokhoven, J. A.; van der Eerden, A. M. J.; Koningsberger, D. C. *J. Am. Chem. Soc.* **2003**, *125*, 7435.
(50) Bothe, J. V.; Brown, P. W. *J. Am. Ceram. Soc.* **1993**, *76*, 2353.
(51) van Donk, S.; Janssen, A. H.; Bitter, J. H.; de Jong, K. P. *Catal. Rev.* **2003**, *45*, 297.
(52) Gilson, J.-P.; Edwards, G. C.; Peters, A. W.; Rajagopalan, K.; Wormsbecher, R. F.; Roberie, T. G.; Shatlock, M. P. *J. Chem. Soc., Chem. Commun.* **1987**, 91.
(53) Brunner, E.; Ernst, H.; Freude, D.; Fröhlich, T.; Hunger, M.; Pfeifer, H. *J. Catal.* **1991**, *127*, 34.
(54) Sanz, J.; Fornés, V.; Corma, A. *J. Chem. Soc. Faraday Trans.* **1988**, *84*, 3113.
(55) Woolery, G. L.; Kuehl, G. H.; Timken, H. C.; Chester, A. W.; Vartuli, J. C. *Zeolites* **1997**, *19*, 288.
(56) van Bokhoven, J. A.; Koningsberger, D. C.; Kunkeler, P.; van Bekkum, H.; Kentgens, A. P. M. *J. Am. Chem. Soc.* **2000**, *122*, 12842.
(57) Hunger, M. Catalytically Active Sites: Generation and Characterization. In *Zeolites and Catalysis: Synthesis, Reactions and Applications*; Cejka, J., Corma, A., Zones, S., Eds.; Wiley-VCH: Weinheim, 2010; Vol. *2*, pp 493−546.
(58) van der Bij, H. E.; Weckhuysen, B. M. *Phys. Chem. Chem. Phys.* **2014**, *16*, 9892.
(59) Wu, P.; Komatsu, T.; Yashima, T. *J. Phys. Chem.* **1995**, *99*, 10923.
(60) Chen, N. Y.; Smith, F. A. *Inorg. Chem.* **1976**, *15*, 295.
(61) Jiao, J.; Altwasser, S.; Wang, W.; Weitkamp, J.; Hunger, M. *J. Phys. Chem. B* **2004**, *108*, 14305.
(62) Menezes, S. M. C.; Camorim, V. L.; Lam, Y. L.; San Gil, R. A. S.; Bailly, A.; Amoureux, J. P. *Appl. Catal., A* **2001**, *207*, 367.
(63) Chevreau, T.; Chambellan, A.; Lavalley, J.; Catherine, E.; Marzin, M.; Janin, A.; Hemidy, J.; Khabtou, S. *Zeolites* **1990**, *10*, 226.
(64) MacKenzie, K. J. D.; Temuujin, J.; Smith, M. E.; Angerer, P.; Kameshima, Y. *Thermochim. Acta* **2000**, *359*, 87.
(65) Oehler, J. *Nature* **1973**, *241*, 64.
(66) Flörke, O. W.; Langer, K. *Contrib. Mineral. Petrol.* **1972**, *36*, 221.
(67) Aouali, L.; Teanjean, J.; Dereigne, A.; Tougne, P.; Delafosse, D. *Zeolites* **1988**, *8*, 517.
(68) Pellet, R.; Casey, D.; Huang, H.; Kessler, R.; Kuhlman, E.; Oyoung, C.; Sawicki, R.; Ugolini, J. *J. Catal.* **1995**, *157*, 423.
(69) Peixoto, D. P. B.; Cabral de Menezes, S. M.; Pais da Silva, M. I. *Mater. Lett.* **2003**, *57*, 3933.
(70) Kim, W.-G.; Kim, N.-H.; Kim, J.-H.; Seo, G. *Korean J. Chem. Eng.* **1999**, *16*, 392.
(71) Caeiro, G.; Magnoux, P.; Lopes, J. M.; Ribeiro, F. R.; Menezes, S. M. C.; Costa, A. F.; Cerqueira, H. S. *Appl. Catal., A* **2006**, *314*, 160.
(72) Roberge, D. M.; Hausmann, H.; Holderich, W. F. *Phys. Chem. Chem. Phys.* **2002**, *4*, 3128.
(73) Kooyman, P. J.; van der Waal, P.; van Bekkum, H. *Zeolites* **1997**, *18*, 50.
(74) Müller, M.; Harvey, G.; Prins, R. *Microporous Mesoporous Mater.* **2000**, *34*, 135.
(75) Beers, A.; Van Bokhoven, J.; De Lathouder, K.; Kapteijn, F.; Moulijn, J. *J. Catal.* **2003**, *218*, 239.
(76) Blasco, T.; Corma, A.; Martínez-Triguero, J. *J. Catal.* **2006**, *237*, 267.
(77) van der Bij, H. E.; Meirer, F.; Kalirai, S.; Wang, J.; Weckhuysen, B. M. *Chem. Eur. J.* **2014**, *20*, 16922.